Galactic Emission Mapping

James M. Lamb

Physics Senior Thesis

Advisor: George Smoot

University of California, Berkeley

May 17, 2002

Contents

Abstract

An analysis of a 2.3GHz sky survey is presented. Special attention is paid to calibration techniques and baseline contamination. Current data is found to be lacking, but the analysis points out improvements that can and should be made to the experimental procedure.

1 Introduction

Understanding of the emission of the galaxy is important both for its property as a foreground in any measurement of the Cosmic Microwave Background, and for study of astrophysical processes. CMB foreground extraction depends upon accurately knowing the frequency spectra of the foreground, the spatial dependence of the frequency spectra, and the spatial power spectra of the foreground (Tegmark 1999 [5]). Though it has been shown that foreground removal is achievable for upcoming CMB mapping experiments ([5],Knox 1998 [7]), that determination depends on near-perfect prior knowledge of the aforementioned parameters.

Diffuse galactic emission comes from synchrotron, free-free, and dust processes (see Figure 1).

The frequency spectrum of free-free emission is well known as a power law, but its spatial dependence and absolute level are not, because it is not the dominant emission at any frequency [5]. At frequencies where free-free might exceed synchrotron radiation, adequate galactic surveys do not exist (De Zotti et al 1999, [9]).

Dust emits as a blackbody modified by a power-law emissivity ($J_\nu \propto \nu^\beta B(\nu)$) . Interstellar dust is heated by infrared radiation to about 18-20K (Longair [**?**]).

Synctrotron emission is the dominant high-latitude galactic emission up to 5-10GHz [9]. The spectral index β ($J_\nu \propto \nu^\beta$) of synchrotron emission has been shown to vary both spatially and with frequency (Platania et al 1998 [10]). Because of this, thorough characterization of synchrotron radiation at several frequencies would be beneficial. Synchrotron emission arises from ultrarelativistic electrons being accelerated in magnetic fields. If the magnetic field is B, and the energy spectrum of electrons is $N(E)dE = N_0 E^{-p}$, then the intensity of synchrotron radiation is $J_\nu \propto N_0 B^{(p+1)/2} \nu^{-\beta}$, where the spectral index β is given by $\beta = (p-1)/2$. Thus characterization of synchrotron radiation could help constrain the value of the galactic magnetic field and the underlying electron energy spectrum and its sources.

A survey of galactic emission should have the following qualities:

1. **Accurate Gain Calibration.** Error in receiver gain will show up as uncertainty in the range of antenna temperature over a map.

2. **Accurate determination of zero-level (minimum temperature).** Any attempt to compare maps at different frequencies to extract spectral index information or extrapolate to higher frequencies will depend on accurate knowledge of the absolute level of emission. Zero-level determination depends on accurate calibration of receiver noise temperature. Excessive baseline errors may also force abandonement of absolute zero-level calibration.

3. **Control of baseline errors.** Low-frequency (1/f) noise in the time-ordered data can show up as artifacts ("stripes") in the data in map form, depending on scan pattern. At best, low frequency noise will show up as increased statistical uncertainty in a map. Ground contamination, if present, will always show up as map artifacts.

4. **Full sky coverage.** Full sky coverage is usedful for determining the spatial power spectra of emission [9].

A couple of full-sky surveys that meets these criteria do exist, including the canonical Haslam 408 MHz survey (Haslam et al 1982 [13]) and a survey at 1420MHz (Reich and Reich 1988 [14]; Testori et al 2001 [19]), but additional frequency coverage would be beneficial. Maps have been attempted at higher frequencies (notably including at 2326MHz by Jonas et al 1998 [15]), but none have been totally successful in meeting the criteria. The Galactic Emission Mapping (GEM) project was begun in order to overcome these shortcomings.

The present data at 2.3 GHz does not live up to that expectation. However, this analysis can point out shortcomings so that future data-taking can be more successful.

The analysis covers a total of 542.9 hours of data was taken in Brazil, from Cachoeira Paulista (lat=-22.6835, lon=-44.9984, 572 m.a.s.l) in May, June, and November 1999, and an additional 159.3 hours of data taken from a site in Colombia (lat=5.6188, lon=-73.5835, 2,173 m.a.s.l).

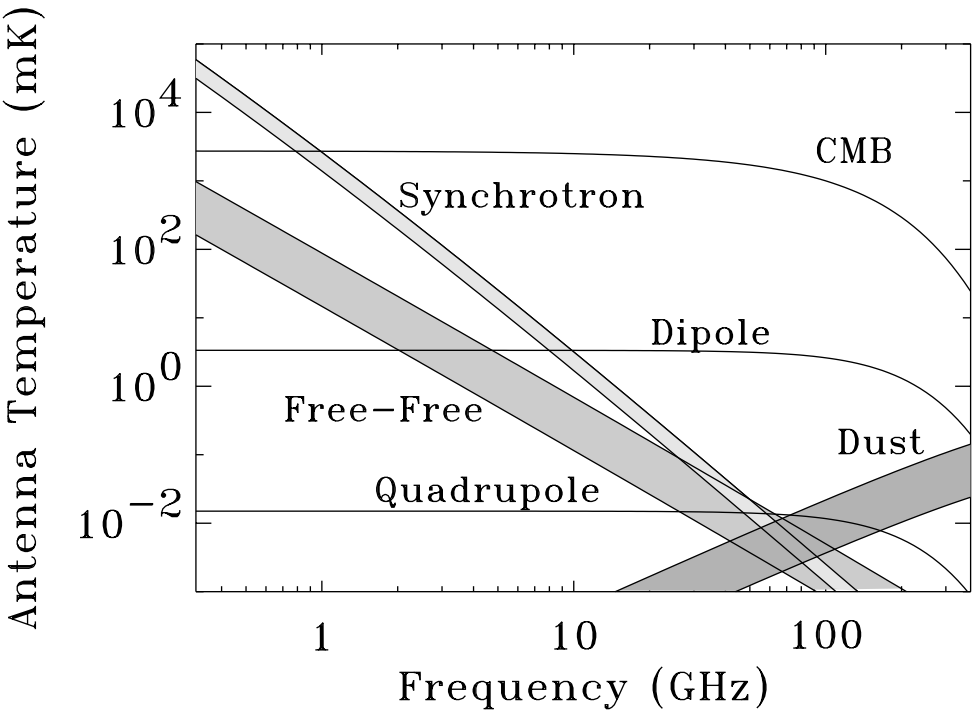

Figure 1: Galactic emission, compared to approximate CMB levels. Figure taken from [10]

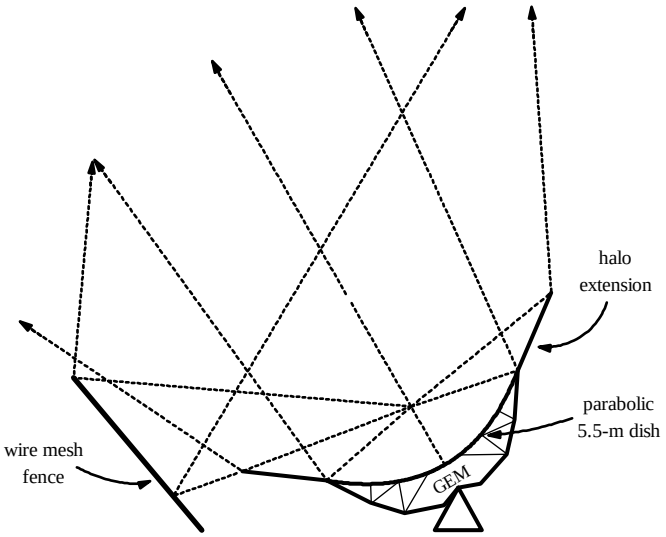

Figure 2: GEM dish schematic, showing ground screens and halo shields.

2 Apparatus

2.1 The Antenna

The GEM apparatus consists of a 5.5 meter symmetric parabolic dish that is semi-portable and into which can be swapped a variety of receivers with a minimum of effort. This design was chosen to meet the goal of large-area surveys (requiring data taken from different latitudes) at a variety of frequencies, taken using one telescope to aid calibration.

The dish has freedom to rotate continuously in azimuth, and can safely be pointed at zenith angles up to 45 degrees. The nominal angular resolution at 2.3 GHz is given by $1.22\frac{\lambda}{D} = 1.652^{\circ}$. The dish is extended by halo shields, and surrounded by a wire-mesh fence, to keep out diffracted signal from the ground (see Figure 2).

During scans of the sky, the beam axis is kept at a constant zenith angle (approximately 30 degrees in these data). The dish is then repeatedly scanned through all 360 degrees of azimuth. In this way a 60 degree declination band is observed, centered on the local zenith of the site. One advantage of this scan pattern in that constant amount of atmosphere is kept as a foreground, reducing the effect of atmospheric emission.

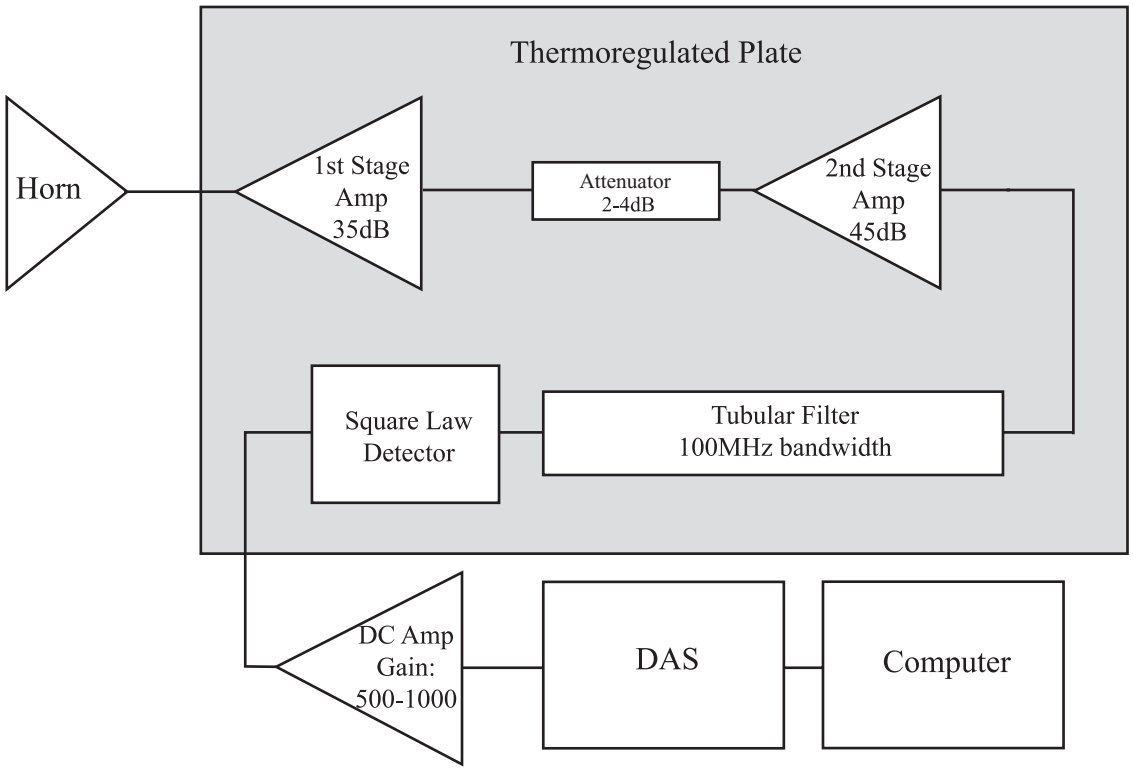

Figure 3: Schematic diagram of 2.3 GHz Receiver.

2.2 The 2.3 GHz Receiver

The 2.3 GHz total-power receiver, which was built and tested by Marco Bersanelli, uses a HEMT first-stage amplifier for low system noise. The receiver uses several stages of RF amplification, followed by a square-law detector and integrating DC amplifier (see Figure 3). The signal integration time is 0.56002 seconds.

The receiver voltage, along with ambient temperatures and other housekeeping data, is sampled by the 16-channel, 16-bit Data Acquisition System (DAS). The data is packaged in "frames", and sent to a computer at a rate of one per integration time. The dish is outfitted with a noise-source that fires four frames out of every 80. The noise-source was supposed to provide a means of relative gain calibration, but we found it to be unreliable.

The RF chain and detector diode are temperature-regulated using a two-stage system. The receiver is integrated into a small insulated box cooled below ambient temperature using a Peltier device. The RF chain sits on a large aluminum plate, whose temperature is regulated using power resistors. The regulation uses a

proportional-control system rather than hysteresis about the set point, to minimize oscillations.

3 Data Analysis

3.1 Introduction

Very briefly, the analysis of GEM data can be summed up in the following three questions. Where are we looking? Are we sure we're not seeing something else too? How do we convert receiver voltage output into sky brightness temperature? In other words, the analysis can be grouping into the following three categories: Pointing calibration, noise removal, and determination of the system parameters gain constant and receiver temperature. I present the analysis in an order I find conceptually linear. The actual analysis was not so linear; for example, some noise removal must be done before system parameters are determined, but system parameters must be determined before temperature-correlated noise can be removed (further explanation can be found in the data analyis flow chart in Figure 4).

3.2 Pointing Calibration

The azimuth angle of GEM is recorded by an optical angle encoder. The zenith angle is kept rigidly fixed. The first step in pointing calibration is interpreting the output voltage of the azimuthal encoder as an angle. Nominally, the encoder outputs an analog voltage from zero to ten volts, in 4096 discrete steps. However, due to manufacturing imperfections and degradation of the components with time, the maximum output varies from 10 volts. To make the conversion from encoder voltage to azimuthal angle, it is necessary to know this maximum output (V_{max}).

Finding V_{max} might seem like a trivially easy task, but the situation is complicated by the fact that V_{max} is never actually a recorded output of the encoder. The encoder is run such that the encoder voltage decreases monotonically to zero, and then rises to V_{max} very rapidly. Due to capacitive coupling in the few meters of wire between the encoder and the DAS, combined with the rapid rotation speed of the dish (1 rpm), the DAS end of the encoder output line never reaches V_{max}. In other words, the RC time constant of the line is longer than the time it takes the encoder to sweep off the peak azimuth value. V_{max} is found through extrapolation, using the average amount

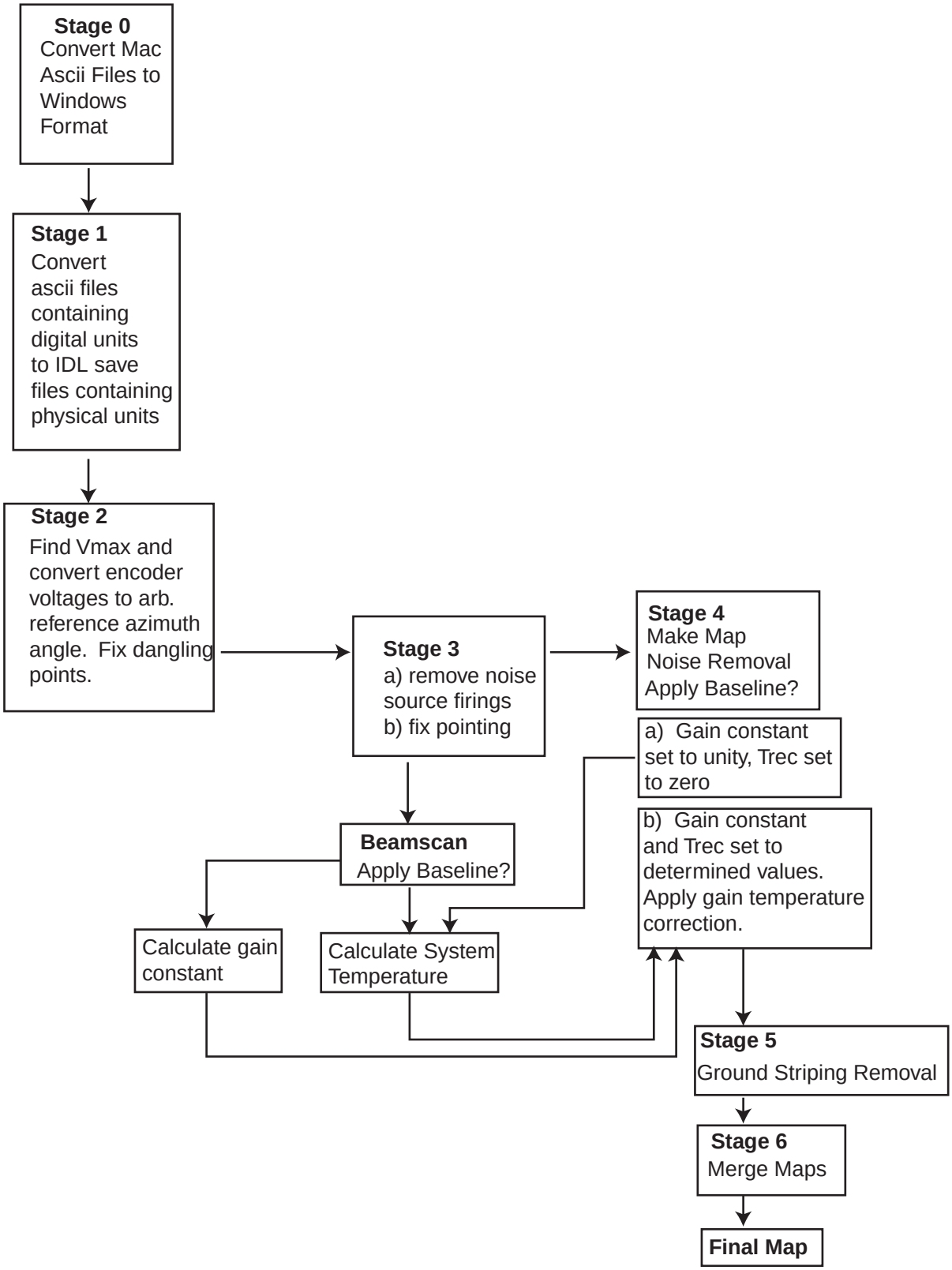

Figure 4: GEM data analysis Pipeline.

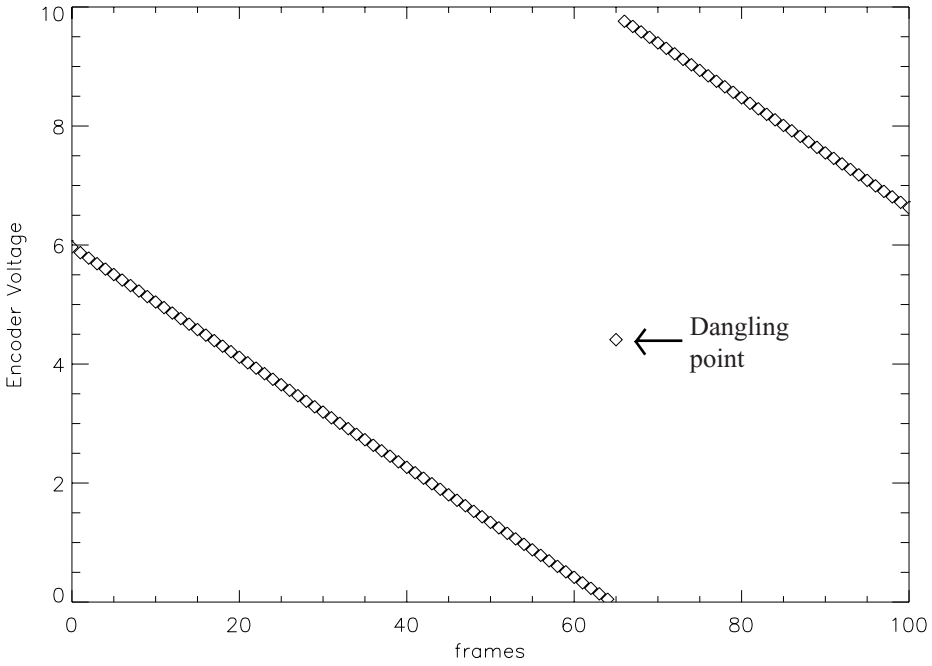

Figure 5: Encoder voltage, showing dangling point

of voltage swept through by the encoder during one integration time. This process is done for every rotation during data-taking, and the value is averaged.

Once voltage is converted to angle, a constant must be added to the angle in order to referece it to the true azimuth angle. This azimuth offset is found by observing the receiver voltage peak as the beam crosses either the sun or the moon. Because of the discrete nature of the signal due to integration, a gaussian is fit to the signal as a function of azimuth, and the azimuth at which the signal would have peaked is compared to the azimuth of the object at that time. A similar procedure is done to find the true elevation of the beam, using the peaks in the signal every rotation as the target transits the elevation of the beam.

We established Brazil data pointing using four transits of the sun across GEM's zenith, and 14 transits of the moon. This gave us about 75 useful peaks from the sun and 30 from the moon to determine azimuthal pointing, and three and eight peaks respectively to establish GEM's constant zenith angle. Azimuthal pointing was established to within an error of 0.24 degrees. The zenith angle was determined to be 29.87 ± 0.19 degrees. We used fewer moon transits for the zenith determination because for some transits, not enough of the azimuthal crossings of the moon by the beam lay above the noise floor to get a convergent gaussian fit (particularly when the

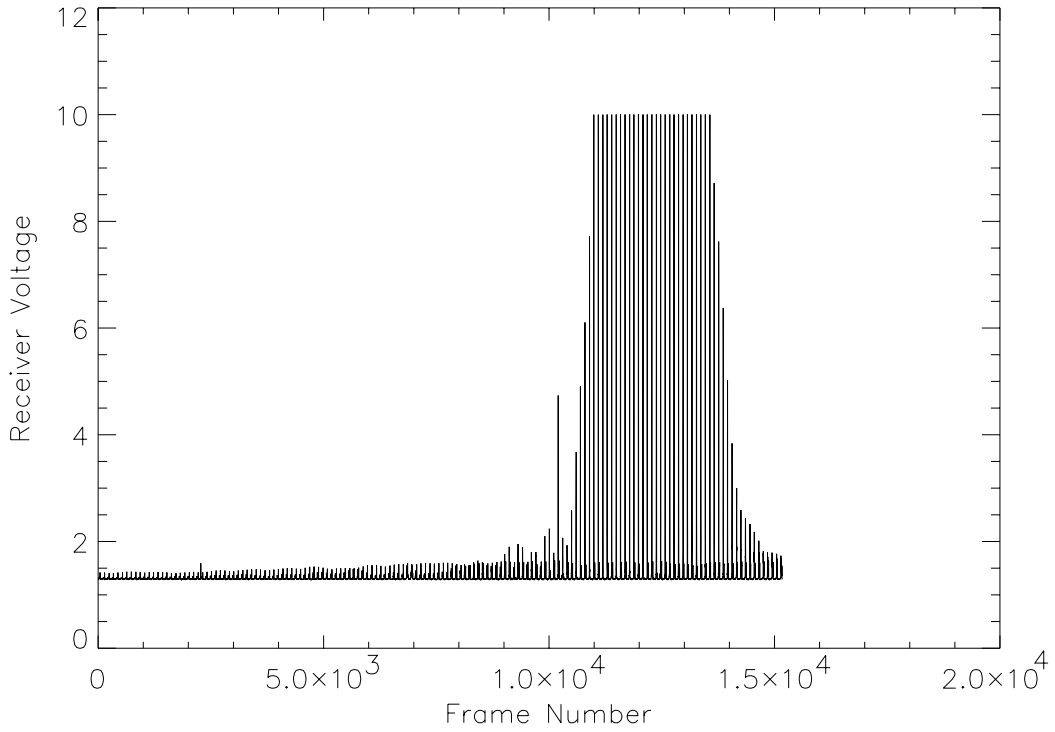

Figure 6: Signal showing transit of sun past GEM's zenith angle. Notice the saturation of the signal. This is due to the DC signal rising above the reference voltage of the DAS analog-to-digital converter, not to saturation of the RF or DC amplifiers.

signal included the galactic plane or radio-frequency interference). We had the same trouble with one of the sun transits, because the signal made too rapid a transition from being below the noise floor to being saturated.

We established Colombia data pointing using four crossings of the sun. We determined azimuthal pointing to within 0.13 degrees. We found the zenith angle to be 30.32 $\pm$ 0.06 degrees. Our moon ephemeris generation was done using code published by Joe Heafner [2] to interpret the JPL ephemeris data. It was found to differ from JPL Horizons online ephemeris [16] by less than 0.01 degrees. Our sun ephemeris data was done using *Sunpos* from the IDL Goddard library [17]. *Sunpos* was found to differ from Heafner's code by less than 0.1 degrees, which in turn differed from JPL Horizons by less than 0.001 degrees.

3.3 Noise Removal

Not all of the data are useful, due to systematic noise. Our first look at the data in map form is presented in Figure 7. The only cuts on the data to produce the map were cuts to remove data when the beam was close to the sun ($\leq$ 30 degrees) and moon ($\leq$ 3 degrees), and cuts to remove the frames where the noise source fired. The sun and moon cuts removed a total of 12.36 hours of data. Noise source firing cuts removed 40.07 hours of data.

The noise observed in GEM can be put into four categories: structured Radio-frequency interference (RFI), unstructured RFI, ground contamination, and baseline contamination.

3.3.1 Structured RFI

Structured RFI exists in the data in the form of a semi-constant high-amplitude signal from a well-defined azimuth region. As such, the RFI is easily identified as having an earthly origin. The azimuth region containing the RFI, as well as a small buffer region, was cut from the data. The origin of the signal could be a radio tower in a nearby town (the tower was put up after the GEM project chose the site).

3.3.2 Unstructured RFI

Unstructured RFI makes its appearence in the data as spikes nearing ten volts in amplitude. The RFI probably originated with the use of a microwave oven by the

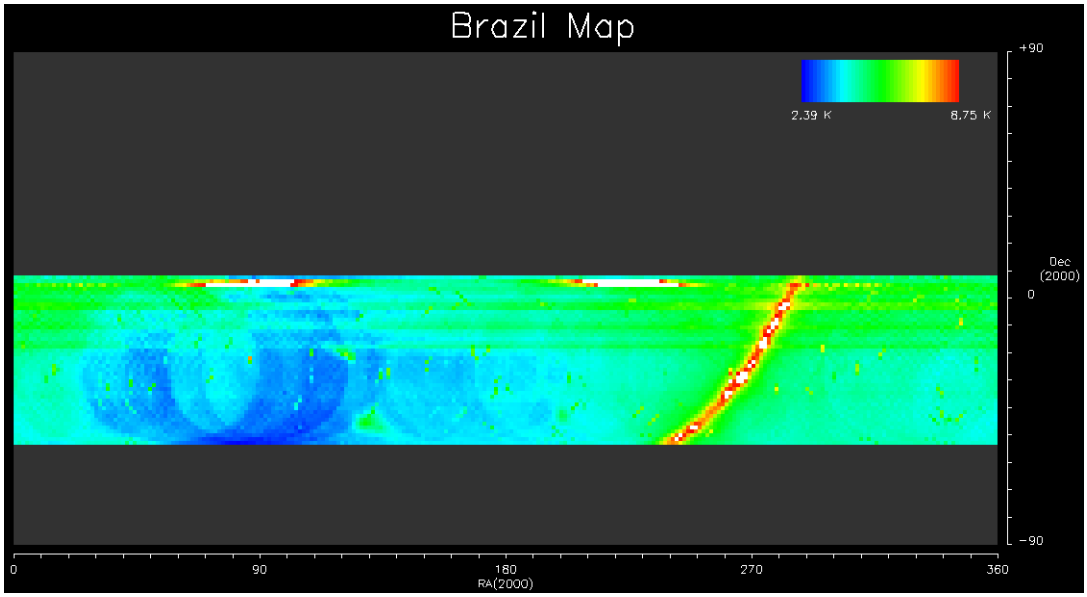

Figure 7: Data in map form, after only sun, moon, and noise source cuts. The features at right ascension 90 and 220, declination near zero, are structured RFI. The poor baseline of the map is due mostly to HEMT temperature variations.

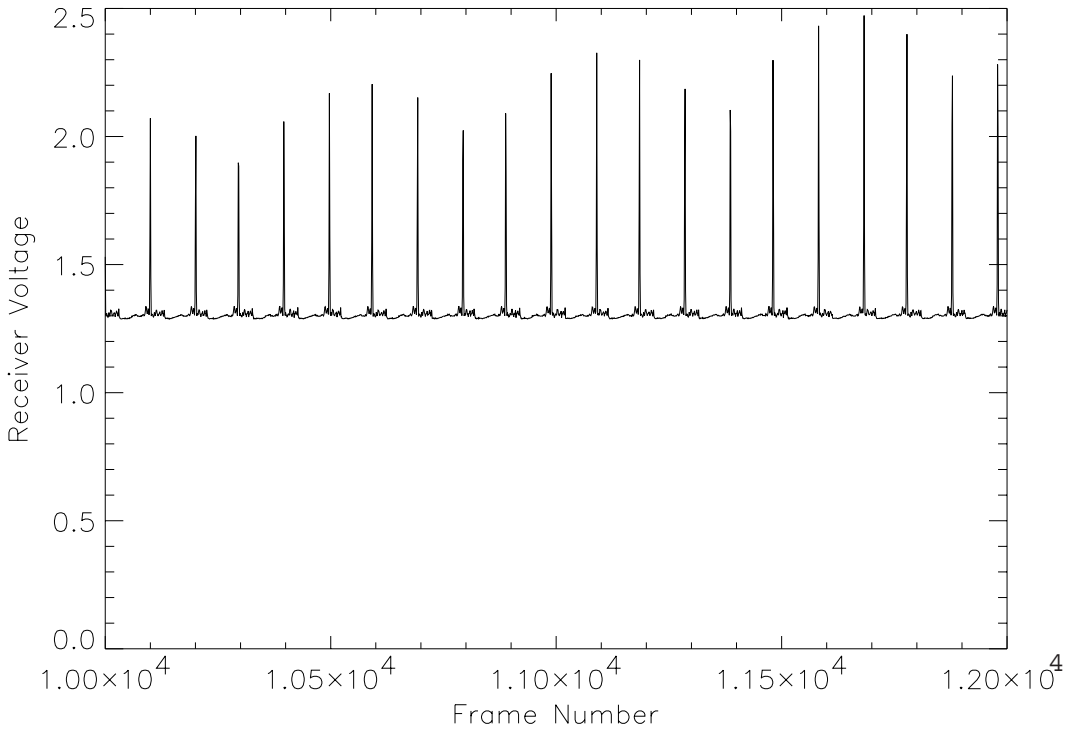

Figure 8: Signal showing structured RFI

data-taking personnel. It is easily removed with a three-sigma cut after the data is put into right-ascension and declination bins.

3.3.3 1/f noise

Thermally induced instabilities in the equipment and intrinsic instabilities in transistor gain produce long-timescale spurious signal variations. These variations show up as "striping" when the data is put into map form. We have tried (or will try) a number of methods to get rid of the stripes.

The first step in removing the baseline is to correct for fluctuations in receiver gain that can be correlated with physical temperature. The expected signal, when the receiver is looking at a constant sky load, can be broken up as follows:

$$S(T_{phys}) = G(T_{phys})T_{sys}(T_{phys}) = [(G + \Delta G(T_{phys})]\,[T_{sys} + \Delta T_{sys}(T_{phys}])$$

It is expected that the gain will fall as temperature rises, and T_{rec} will increase as physical temperature rises, in an approximately linear fashion. We used data from one of the regions ($36 \leq \alpha \leq 60, -34 \leq \delta \leq -22$) identified by Tony Banday as a "cold sky" region to measure the correlation. The data clearly exihibit a linear relationship with negative slope, so we neglect variations in T_{rec} with respect to T_{phys}. We assume that the effect of temperature on gain can be linearized over the range of interest, giving:

$$m\Delta T_{phys} = \Delta S(T_{phys}) = \Delta G T_{sys}$$

$$\Delta G = \left(\frac{1}{T_{sys}}\right) m$$

$$g = \frac{1}{G} = \frac{1}{1 + \frac{g_0 m \Delta T_{phys}}{T_{sys}}}$$

where G_0 is the gain at a reference temperature (the mean temperature over which the gain constant was determined from the moon), and ΔT_{phys} is the temperature difference from this reference. The slope m of the signal with respect to temperature was measured to be $-0.022 \pm 0.0026 VK^{-1}$.

This method partially reduces baseline variation. It is most effective against long-timescale temperature variations, such as those caused by saturation of the temperature regulation system. The temperature regulation system saturates when the

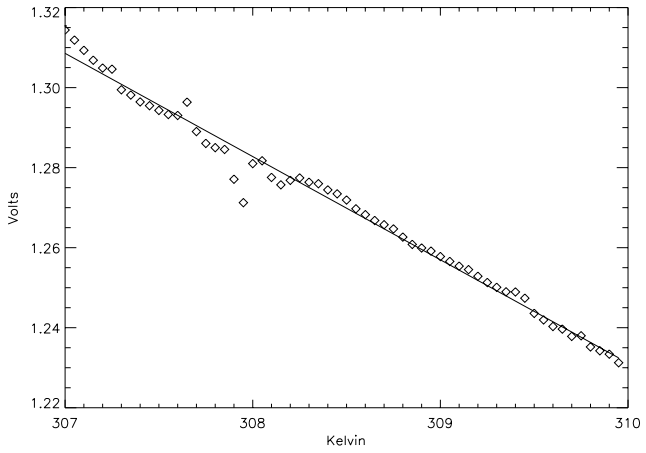

Figure 9: Signal as a function of HEMT temperature, while looking at cold sky. Showing line fit to data.

ambient temperature overrides the Peltier device and forces the RF plate above the set point for minimum heater resistor current. See Figure 10a for a map showing the effects of applying this temperature correction.

3.3.4 Artificial Baseline Correction

In the case where baseline correction is not possible using the above method, an artificial baseline subtraction can be made. The crux of the method used is the assumption that every GEM scan should see the same minimum temperature. While this is obviously not strictly true, we believe it to be a fair approximation because the wide (60 degree) GEM scans, even when centered on the galactic plane, reach high galactic latitudes. The procedure for doing artificial baseline correction is to identify the minimum temperature in each rotation in the time-ordered data. A cubic spline is then fit to and subtracted from the data, zeroing the minimum temperature over each scan. A constant is added to the data, to renormalize the minimum temperature to the expected value (2.73 K).

Cubic splines are prone to oscillation. We tried to minimize oscillations by ensuring that per-rotation minimums were approximately evenly spaced, at about fifty frames separation. In separating data into "rotations", there is some degree of freedom in what is defined as a rotation. Because most of the lowest signal values lie in low declination bands, minima typically occur near zero and 360 degrees, so the data was binned into rotations such that this region lay in the middle of the rotation,

(a)

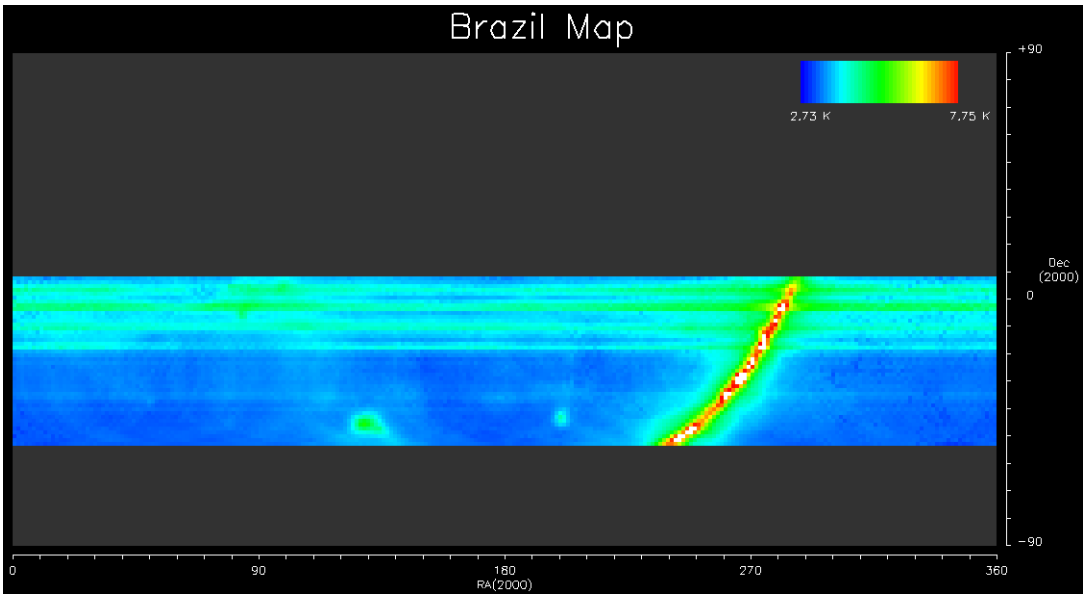

(b)

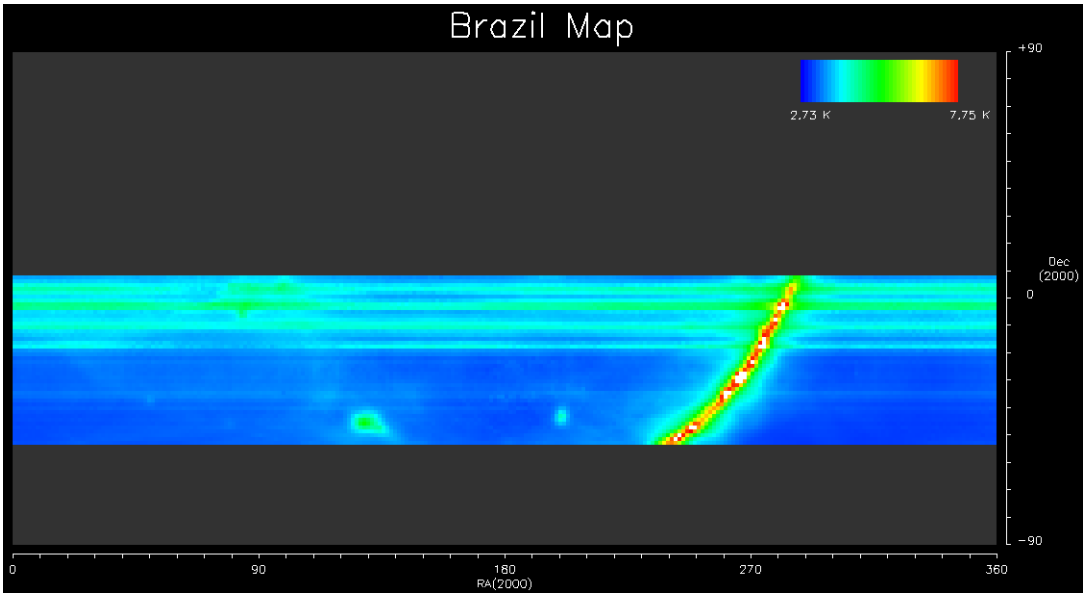

Figure 10: Maps after correction for temperature susceptibility of gain (a), and after temperature correction and spline baseline subtraction (b).

ensuring that minima did not occur close together in time order. In the case that minima did lie close together in time order, one of the minima was thrown out. See Figure 10b for a map after application of this spline-fit baseline.

The obvious failure of this method is that the minimum temperature seen by each scan is not actually the same. This assumption will damp out very large-scale temperature variations, in effect depressing the signal close to the galactic plane.

There has been much work done on similar effects facing PLANCK Surveyor. Since the scan pattern of PLANCK is fairly similar to that of GEM (both consisting of repeated, overlapping circular scans), a discussion of their planned methods might shed some light on our problems . Their method, first explained in Delabrouille 1998 [8], works on the fact that if a pixel is seen by two separate scan circles (shorthand for scans repeated over the same circular patch of sky), the two scan circles should agree on the value of the sky temperature at that pixel. We can define an error quantity, $(M_1 - {}_1) - (M_2 - A_2)$. Here $M_{1,2}$ are the observed signal from pixels 1 and 2, and $A_{1,2}$ are the additive constants representing the contribution of pink noise. If the constants A are known, the error quantity should vanish, limited only by the uncertainty, due to finite sensitivity, inherent in measurement of a sky region in finite time.

In general the constants A are not known. Instead, they can be found by minimizing the sum of errors over all pixel intersections:

$$S = \sum_{i,j,i \neq j} \sum_{pairs} ((M_i - A_i) - (M_j - A_j))^2_{pair}$$

Here the sum is taken over all pairs of measurements that see the same portion of sky from different circle scans i and j. The quantity is minimized to find the constants A_i for every circle scan. The difference between PLANCK's scan pattern and GEM's scan pattern is that PLANCK makes 120 continuous scans along the same circle before repointing. GEM is continuously repointed by the motion of the earth. The largest amount of time we can say GEM's pointing is constant is the time it takes the local zenith to transit our pixelization size, 1.4 degrees. Only five scans are contained in this time, so each scan circle's determination of a pixel's temperature will be subject to considerable error. An additional problem of this method is the computational difficulty; there will be roughly 1000 scan circles, each overlapping about another 1000 scans, so the total number of terms in the above sum will be $\sim 10^6$.

A more realistic possibility is to adapt the above method as a backwards correction after the spline baseline has been performed. Then we can divide all the data

into scan circles centered on the same zenith, but not necessarily in time order, again in bins one pixelization wide. After the spline baseline, 1/f noise should be removed from a given scan circle, but extra noise will be present spatially in the map. Each scan circle, indexed by its right ascension bin, will have an additive constant based on its minimum temperature relative to the minimum temperature over the whole map. The above minimization procedure can be implemented, but this time with only of ~ 100 scan circles seeing ~ 100 other scan circles. Instead of subtracting 1/f noise, this method will put back into the signal power due to actual variation in the sky temperature.

3.3.5 Ground Contamination

When the Brazil data is viewed as a map, horizontal striping is seen, consisting of declinations bands that appear to have spurious higher antenna temperatures (see Figure 10). Because of the scan pattern of GEM, this striping is likely due to the sidelobes of the horn "seeing" some portion of the ground. The ground, at $\sim 300K$, is hot enough that even far out into the horn pattern, it will contribute significantly compared to the $\sim 1K$ sky.

Systematic noise that is synchronous with the GEM's rotation frequency or its harmonics could show up as horizontal striping in the map. However, it is very unlikely that the striping we see is due to this effect. First, the frequency spectrum to produce the precise effect seen would have to be strange indeed. Second, because data-taking is frequently stopped (typically at least once a day). This would phase-detune the scan-synchronous noise. Several averaged datasets would have a lower level of striping than one continuous dataset. This is not observed. However, we cannot be totally sure that the striping is due to ground contamination because of the different "stationary-signal profiles" seen from data taken in May/June and data taken in November (see Figure 11).

The GEM apparatus was designed with "halo" shields around the dish, and wire mesh screens attached to the ground, to redirect any beam spillover. This was not totally successful, probably due to the fact that the ground screens were made of wire mesh instead of solid metal, and had corroded somewhat since first use. Also, the diameter of the mesh was just marginally small enough to provide sufficient attenuation of ground signal at 2.3 GHz, even when the mesh was new.

The cause of the striping could be structured RFI that is not as well-defined as

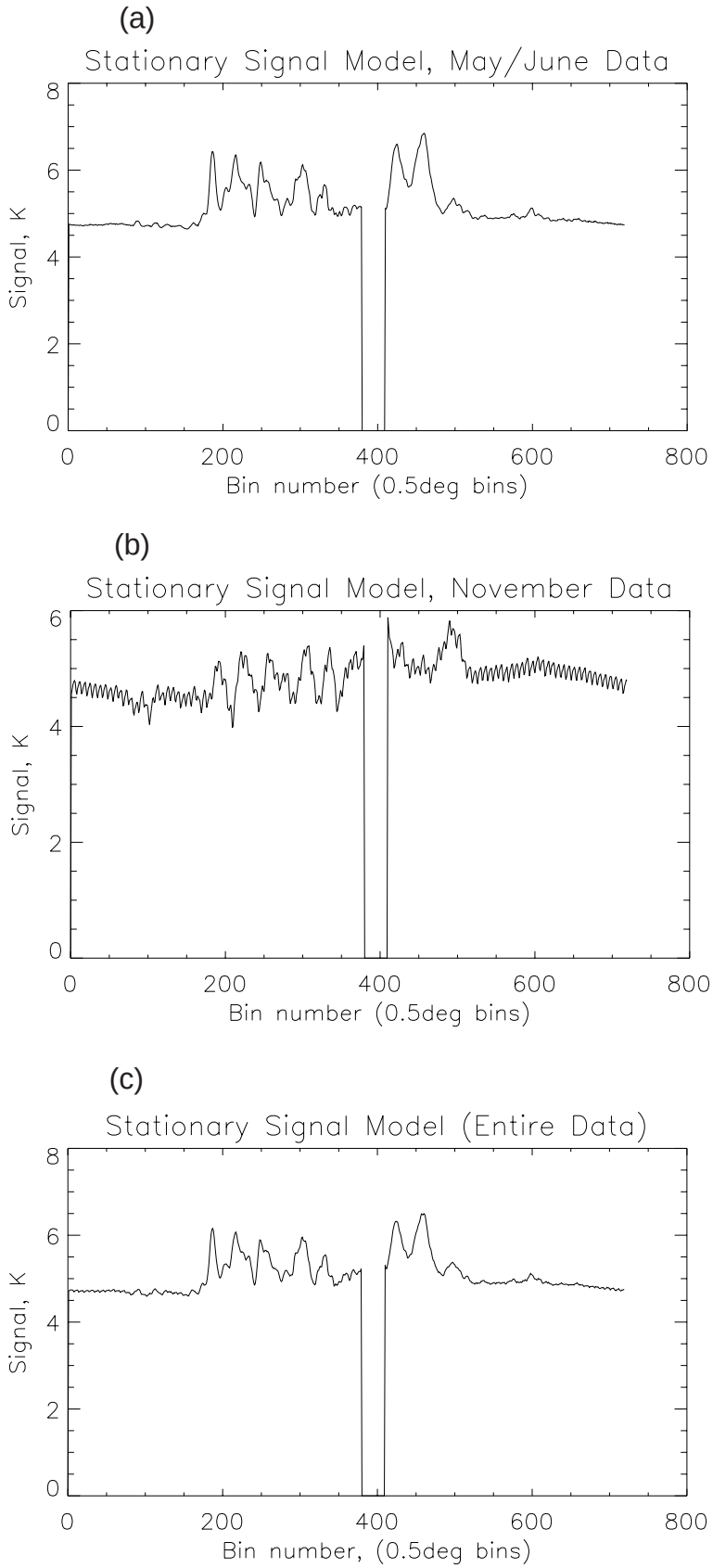

Figure 11: Signal binned by azimuth for (a) May/June data, (b) November data, (c) all data. (c) was the template used to remove azimuth-correlated baseline contamination from the maps.

that mentioned above. In that case, our method of dealing with the striping is only as good as the striping is constant. Alternatively, the ground profile from November data could be different because of the greater dispersion seen in November data (see Figure 18) and the fact that less data was taken in November than in May and June. We have assumed that the contamination is from ground signal or some other stationary signal.

Because each pixel is seen by two azimuths, it is possible to separate ground signal from sky signal. Following the method outlined to remove 1/f noise, the signal at a particular pixel from one azimuth should agree with the signal from the other azimuth, after their relative constants A (representing noise power from ground signal) have been taken into account. The constants A can be determined by least-squares minimization.

$$S = \sum_{\alpha} \sum_{\delta} \left((M^1_{\delta,\alpha} - A^1_{\delta}) - (M^2_{\delta,\alpha} - A^2_{\delta}) \right)^2$$

Each declination band is seen by two azimuths, so A are indexed by δ and an index that is either 1 or 2.

Unfortunately, this summation can be separated by declination band. An infinite number of solutions exist to the linear equations defined by the minimization, because there are two additive constants with only one constraint. If data is taken at more than one zenith angle, so that declination bands are cross-correlated, then this problem will be remedied, aiding ground contamination removal.

Our method of ground-contamination removal is to construct a ground template by binning and averaging all the data by azimuth (see Figure 11), then subtracting the template from the data. This corresponds to setting the constants A equal to the mean value of the signal from the corresponding azimuth bin, averaged over a the full declination band. Physically, this corresponds to assuming that the mean sky temperature over all declination bands is the same. This is approximately true, if we compare to deviation from this assumption to the level of groundstriping seen in the initial maps. The moderate success this affords can be seen from our results (see Figure 12).

3.4 System Parameters

A total-power radiotelescope can be idealized as a linear, noiseless amplifier with some gain G, whose input is a resistor at temperature T_{rec}, representing the noise

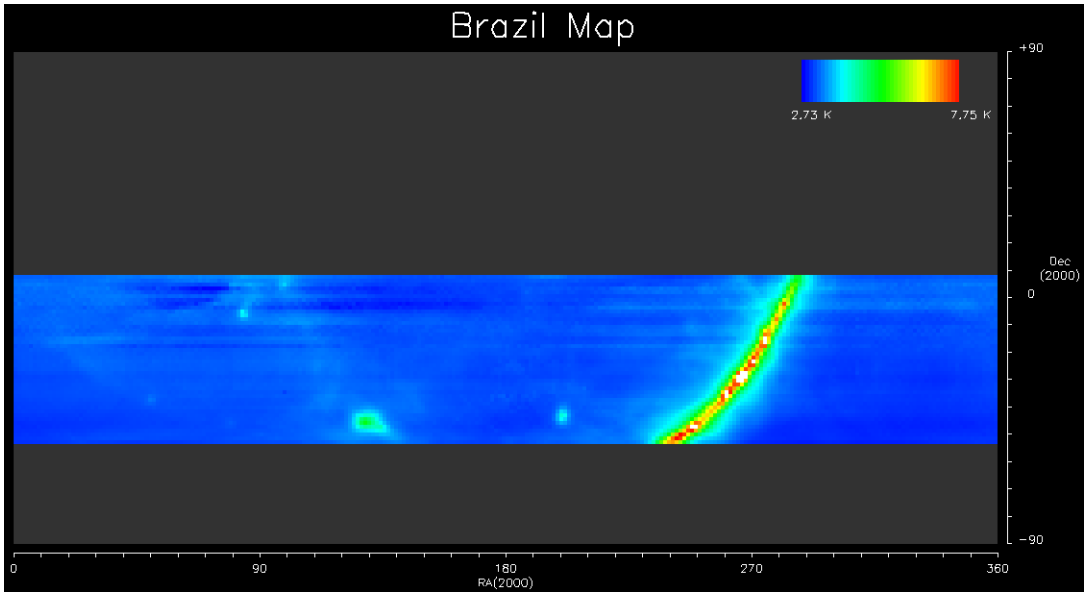

Figure 12: Map of Brazil data after groundstriping has been removed as much as possible. Residual striping is still visible.

power of the receiver, in series with a resistor at temperature T_A, representing the noise power received from the sky. The output of the amplifier is then converted from a power to a voltage by a square-law detector, sent through DC amplification stages, and recorded. The power at the input of the receiver is $k_B T_{sys} \Delta\nu$, where T_{sys} is the combined noise temperature of the sky and receiver, and $\Delta\nu$ is the bandwidth of the receiver. At the output of the (idealized) RF amplification stage the power is $G_{RF} k_B T_{sys} \Delta\nu$. After the detection and DC amplification stages, the voltage recorded will be $G_{RF} G_{DC} C_{det} k_B T_{sys} \Delta\nu$. Here C_{det} is some conversion constant between power input to the detector and voltage output (typically millivolts per microwatt). If we have some voltage S coming from our receiver, we'd probably like to know the corresponding antenna temperature. This can be found by multiplying S by a gain constant $g_c = \frac{1}{G_{RF} G_{DC} C_{det} k_B \Delta\nu}$, and subtracting T_{rec}, the noise power due to the receiver itself. This "gain constant" is not really a gain at all, but a unit conversion that is inversly proportional to the gain.

Fortunately it is not necessary to rely on the nominal values of G_{RF}, G_{DC}, C_{det} and T_{rec}. Both g_c and T_{rec} can be determined experimentally.

3.4.1 Gain Constant

The method we use is a comparision of the observed signal as the beam is centered on the moon with the expected antenna temperature. The expected antenna temperature is given by the following (we use a moon brightness temperature that takes into account the averaging effect of a large beam):

$$T_A = T_m \frac{\Omega_m}{\Omega_b} = g_c S_m$$

Ω_b is the solid angle that would be subtended by the beam, if the beam response function was a step function with height equal to the peak value of the real beam pattern, and had the same integral response. Ω_m expresses the solid angle of the beam subtended by the moon in a similar fashion. Their ratio is a measure of the fraction of the beam power response that "sees" the moon. S_m is the receiver voltage when the beam is centered on the moon.

$$\Omega_m = \int_{obj} P'(\theta, \phi) d\Omega \tag{1}$$

$$\Omega_b = \int_{4\pi} P'(\theta, \phi) d\Omega$$

Where $P'(\theta, \phi)$ is given by:

$$P' = \int_0^\tau P(\theta, \phi, t) dt$$

P' quantifies the non-negligible change in pointing of GEM over an integration time.

To calculate T_A we only need P' and a brightness temperature of the moon. Then to calculate the gain constant we compare T_A with the observed receiver voltage when the beam is centered on the moon (S_m). Both P' and S_m are obtainable by observing the signal when the beam is near the moon.

3.4.2 Beam Pattern

The angular power pattern of a radio-telescope is diffraction-limited, and is given by the fourier transform of the aperature defined by the dish, taking into consideration the illumination of the dish by the feed horn. Analytic solutions exist for a variety of aperature illuminations (see for example Lo and Lee 1993 [3]). However, departures from the ideal modify the functional form of the beam in ways that are extremely hard to quantify analytically. These departures include axial and lateral displacements of

the feed from the focus of the reflector (of even a fraction of a wavelength) [3], the effect of aperature blocking (because the receiver is located at the prime focus), and the effect of the above mentioned change in pointing during one integration.

Thus the ideal solution would be to take enough data that the beam pattern P could be known numerically, and so that the signal when the moon was exactly centered on the beam could be well determined.

Unfortunately, we don't have sufficient data for this. Instead, we use the common approximation of the main beam as a gaussian function to fit the data, and determine P' and the peak response S_m from the fit.

3.4.3 Calculating the Beam Pattern

The natural coordinate system of telescope pointing is the topocentric azimuth-zenith angle system. In order to create a beam pattern, the coordinate system is rotated such that the beam axis is at coordinate $[\theta = 0, \phi = 0]$. Once the coordinates of the moon are rotated by this transformation, the coordinates are projected onto a plane that meets the unit sphere at $[\theta = 0, \phi = 0]$. The projection is defined by $x = \theta sin(\phi), y = \theta cos(\phi)$. The use of a projection is a valid approximation given the very small angles over which the beampattern is nonzero (nominal BWFN 1.652 degrees).

To find the beam pattern, we binned the data by the coordinates of the moon in this beam-centered coordinate system. Before we used the pattern, we threw out any 3-σ outliers to reduce noise. We tried binning the data by 1.5, 1.0, 0.5 and 0.25 degrees. We found the most success by binning by 0.5 degrees (see Figure 13a); smaller binsize resulted in less artificial smoothing, but undersampling occured at 0.25 degrees.

We fit the data to a gaussian of the following form:

$$P(x,y) = A_0 + A_1 e^{-u/2} u = \left(\frac{x - A_4}{A_2}\right)^2 + \left(\frac{y - A_5}{A_3}\right)^2$$

The width is asymmteric because P' will be elongated in the direction of the azimuthal motion of GEM.

3.4.4 Result

The results of fit give the following parameters and errors:

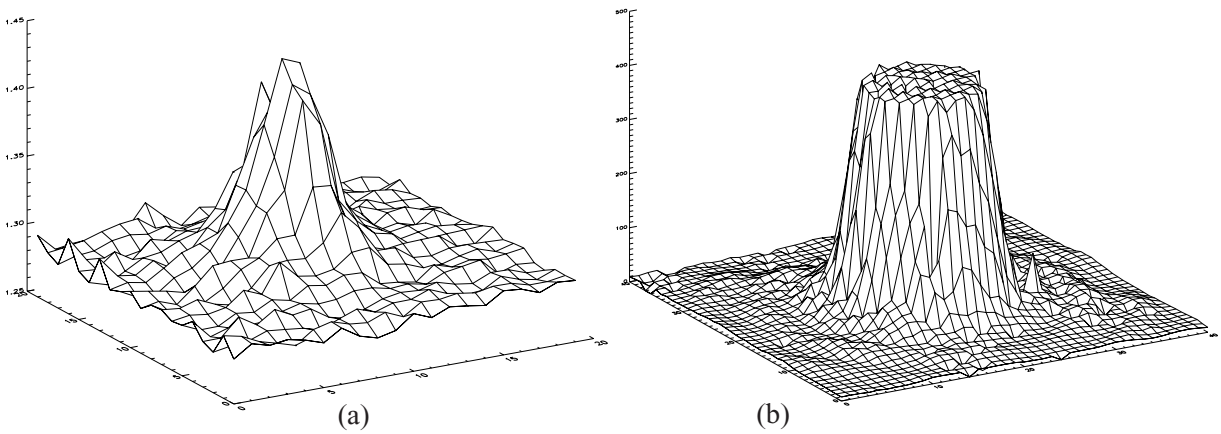

Figure 13: Beam pattern derived from signal's response to the moon (a). Also shown is the signal's response to the sun (b). We tried to fit gaussian and circular-diffraction functions to the sun pattern, but were unable to get a convergent fit.

param	height (V)	x-dir HPBW	y-dir HPBW
value	0.1196	2.46	2.92
frac. error	0.08	0.011	0.008

This gives $\Omega_{beam} = 8.16\pm \sim 2\%$ square degrees and $\Omega_{obj} = 0.21\pm \sim 2\%$ square degrees. We used the results of Krotikov and Pelyushenko (1987) [6] for the radio temperature of the moon. Their value at our wavelength is 225K, with a stated accuracy of $\pm 4\%$. We ignored variation in the temperature with the lunar cycle, because these are small at $\lambda = 13cm$ ($\leq 5K$ from these authors), and obtained our data from an average over many months. We took the angular size of the moon to be the mean value (31.12 arcminutes), and ignored any error associated with this assumption. In determining P', we neglected the widening effect of the convolution of P' with the finite angular size of the moon, and the occultation of the CMB by the moon. We also attempted to find the beam pattern using the sun as a target, but the saturation of the signal far out into the pattern prevents a convergent fit. Additionally, we tried to fit the diffraction pattern of a circular aperature of uniform illumination, but this didn't result in a convergent fit.

We have obtained gain constant $G_c = 48.07KV^{-1}\pm \sim 16\%$. The error on this quantity is due primarily to the uncertainty in the fit.

The beam pattern could be better characterized by doing scans dedicated to observing the moon, at slower azimuthal velocity. The measured beam could be

numerically deconvolved with the moon shape, and if the scans were done on small timescales, the phase and angular size of the moon could be accounted for. This would leave only the radio temperature of the moon as an uncertainty.

3.4.5 Receiver Temperature

The receiver temperature is a constant noise power that is observed independent of any power from the sky. Since the receiver is a linear system, the receiver temperature can be extracted if two objects of known antenna temperature are observed.

If the "hot" antenna temperate T_1 and the cold temperature T_0, and the corresponding receiver voltages are V_1 and V_0 respectively, then the receiver noise temperature T_{rec} is given by (O'Neil 2002, [11]):

$$T_{rec} = \frac{T_0 - YT_1}{Y - 1} Y = \frac{V_0}{V_1}$$

We used the moon as our "hot" temperature, and a cold region of blank sky as the "cold" temperature. T_1 and V_1 take into account the fact that the part of the beam that doesn't fall on the moon, falls on the CMB. We have lumped atmospheric and antenna-emissivity contributions to the signal into T_{rec} (GEM's zenith angle is consant for all scans, and we assume no atmospheric variation).

For the cold sky region, we have used one of the regions ($36 \leq \alpha \leq 60, -34 \leq \delta \leq -22$) identified by Tony Banday 1992 [1] as being the coldest on the sky. These regions are identified as having less than 12K antenna temperature in the Haslam 408 MHz map. Also, there is no evident striping in this region of our map. Thus, with scaling to 2.3 GHz using the factor $\left(\frac{2.3GHz}{0.5GHz}\right)^{\beta}$, with β assumed to be 2.5 (a deliberately conservative value), the temperature of this region due to synchrotron radiation should be less than $0.16K$, a value I take as representative of the error. The error due to the possibility of uncertain free-free and dust emission at this location has been ignored. We believe this to be justified, since synchrotron radiation is the dominant emission at high galactic latitudes up to 5-10 GHz ([9]). But obviously this is not ideal, because it uses prior knowledge of the spectra of the radiation we are trying to measure. The value obtained is $T_{rec} = 57.37K \pm \sim 8\%$

3.5 Merging the Colombia Data with the Brazil Data

Data taken by GEM in Colombia is not of as high quality as data taken in Brazil. The baseline is subject to strange effects. For example, the signal baseline will change by

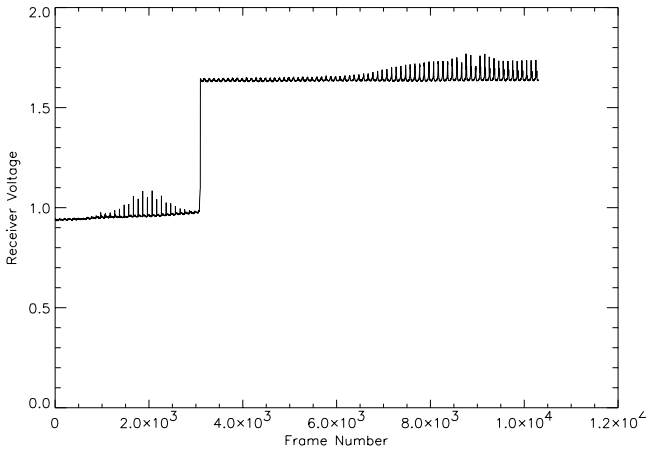

Figure 14: Example of bizarre baseline effects in Colombia data.

0.5 volts over a few tens of frames, being constant for thousands of frames on either side of the jump (see Figure 14).

Sergio Torres, who supervised the data-taking in Colombia, attributed this to unknown electrical problems. Camilo Tello, who supervised the data-taking in Brazil, observed that the feedhorn was axially misaligned during Colombia data-taking. This would degrade the beam pattern even further from a gaussian. We are reluctant to trust the obtained values for both the system parameters (T_{rec} and g_c).

Nevertheless, we think we can gain information by combining the Colombia data with the Brazil data, in order to extend the range of our map and wash out the remains of the striping in the Brazil data. We have done this by calibrating the Colombia data to the Brazil data.

The first step was to subtract a spline baseline from the Colombia data. Then we made a least-squares fit of the Colombia data to the Brazil data, using the Colombia gain constant and and a constant offset as parameters for the fit. (The constant offset takes the place of receiver temperature but has no physical meaning after a spline baseline has been removed.) The fit was made over three declination bands shared by both datasets. These declination bands were chosen because they contained no striping in the Brazil data. The fit gives Colombia gain of $44.13 KV^{-1}$ if a spline baseline is subtracted from the Brazil map used to make the fit, and $46.11 KV^{-1}$ if not. Both combined maps are shown in figure 15. The map using the spline for Brazil data looks better, and the errors are less in Brazil data when a spline baseline is removed. However, there appears to be large angular-scale structure removed from

the map using the baseline (see Figure 15).

As a check on the pointing parameters used for both datasets, a hot region of small angular scale was identified in the shared data. The peak temperature of the region has the same pixel coordinates in both datsets, confirming our pointing (see Figure 16).

4 Sources of Error and Areas of Improvement

The fundamental limit on the certainty of a sky temperature measurement is given by (Kraus [4]):

$$\Delta T_{min} = T_{sys}\sqrt{\left(\frac{1}{\Delta\nu\tau}\right)}$$

Here $\Delta\nu$ is the bandwidth, and τ is the integration time. The term in the root can be thought of as the uncertainty in the number of photons arriving at the detector. Realistically, one must also account for uncertainties in receiver gain.

$$\Delta T_{min} = T_{sys}\sqrt{\left(\frac{1}{\Delta\nu\tau}\right) + \left(\frac{\Delta G}{G}\right)^2}$$

The second term in the root arises from the fact that uncertainty in gain at any given time is indistinguishable from a change in system temperature. (This is not the same thing as error in the determination of the gain). In general we would like this uncertainty to be limited by the fundamental uncertainty, the first term. Unfortunately, this is not the case for GEM. Using the nominal 100MHz bandwidth and $T_{rec} = 55K$, $\frac{\Delta T}{T}$ should be about $7mK$ per sample. The mean number of hits per pixel is about 250, so the statistical error on any given pixel should be about $0.5mK$. The minimum errors on our map are typically a factor of 10 higher (see Figure 17b). We might suppose that the difference is made up by 1/f noise in the gain. It is worthwhile to look at a map of the error of pixels. Figure 17 shows both a statistical error ($\frac{\sigma}{\sqrt{(N)}}$ and simply σ, the latter because $\frac{\sigma}{\sqrt{(N)}}$ significantly underestimates errors if gaussian statistics aren't obeyed. Figure 17 shows a map of σ over the Brazil data, when no spline baseline was removed, and a map of σ over the combined Brazil-Colombia map.

The error maps show several interesting features. First, they highlight the residual ground striping even after cleaning. The circular feature centered at $\alpha = 230, \delta = -30$ could be because the sun-beam data-cut angle, 30 degrees, was not large enough.

(a)

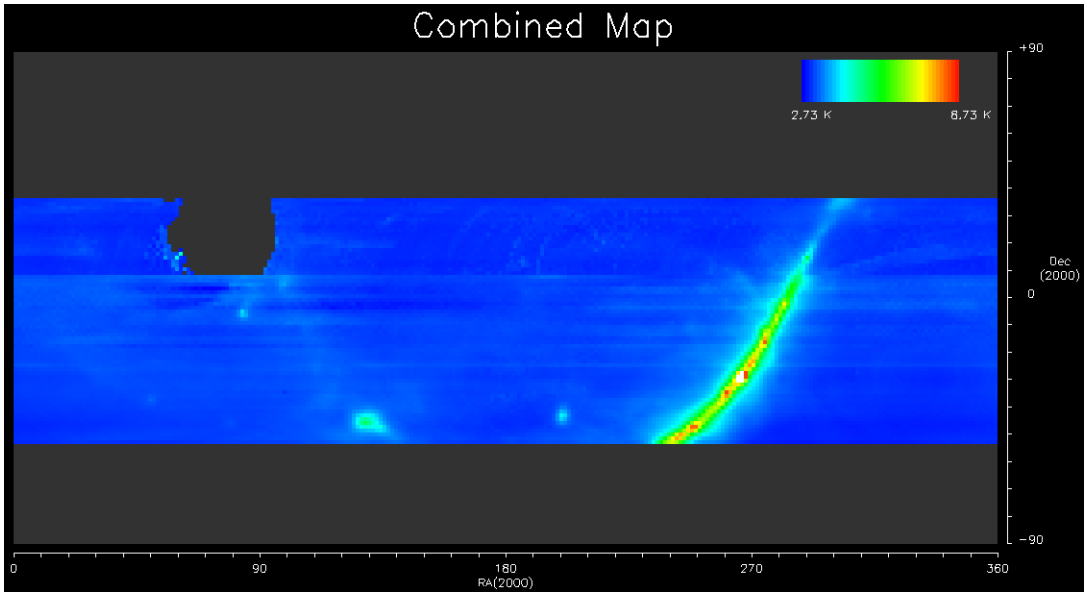

(b)

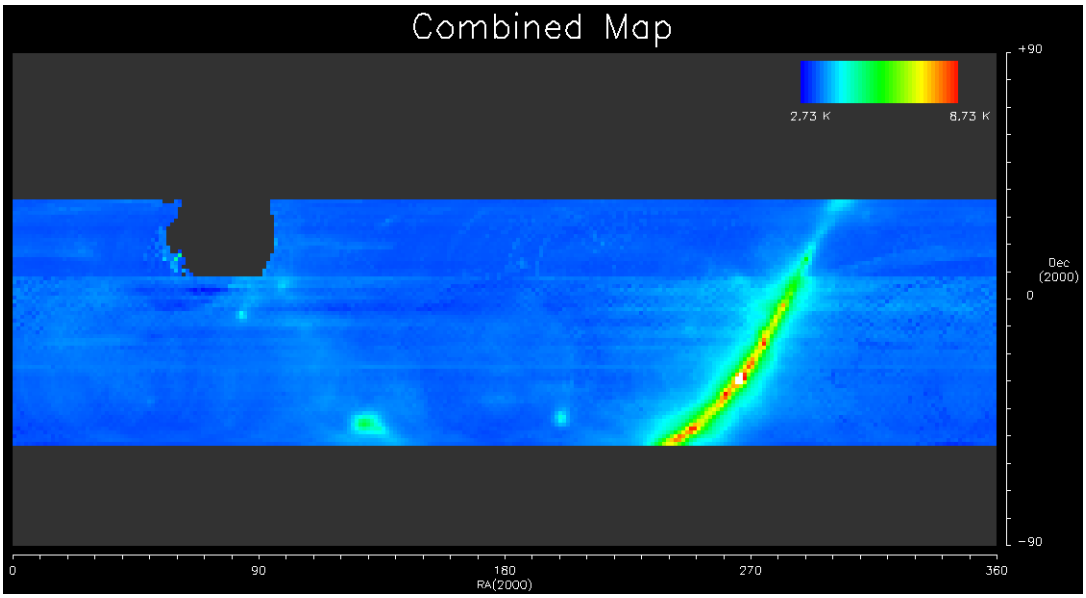

Figure 15: Combined Brazil and Colombia maps, using baseline (a), and not (b).

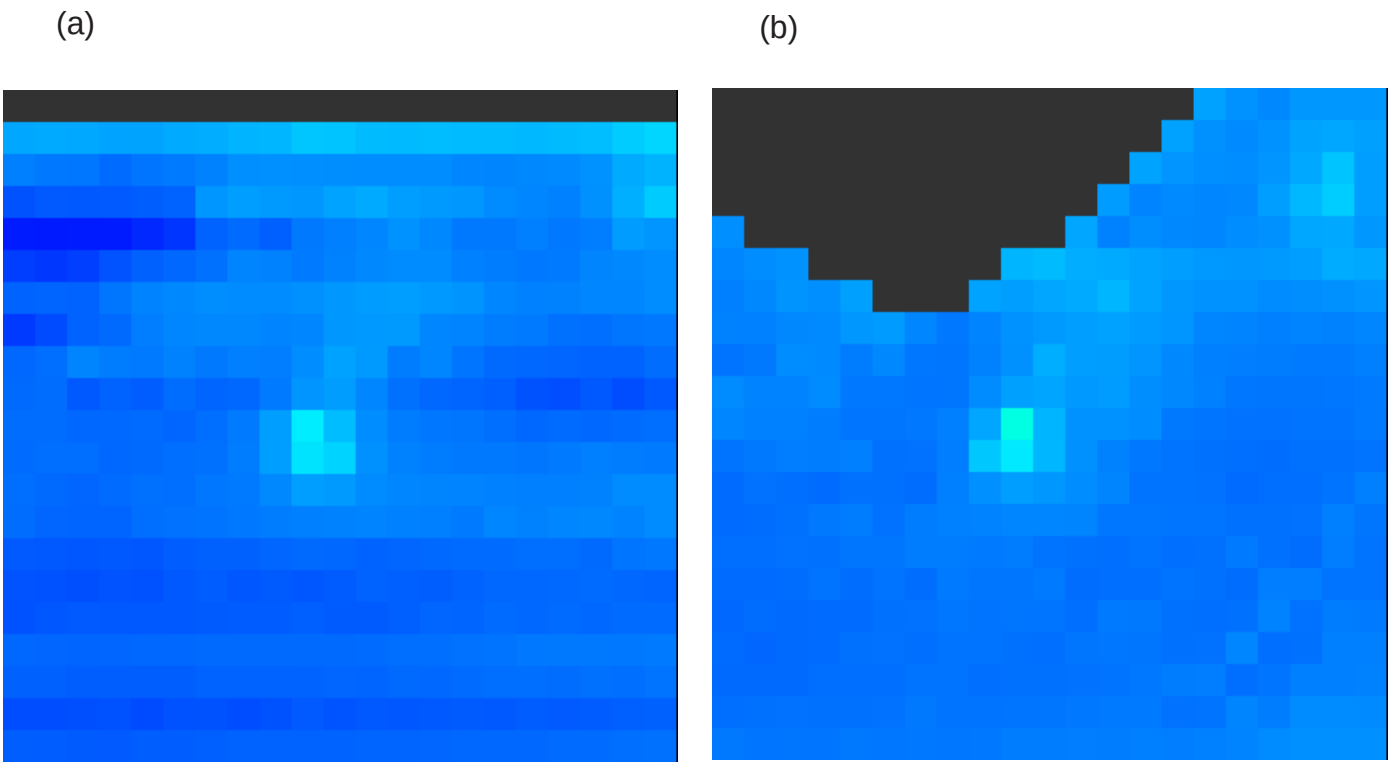

Figure 16: Feature at approximate coordinates right ascension 90 degrees, declination zero. Seen from Brazil (a) and Colombia (b) at same coordinates, confirming pointing.

(a)

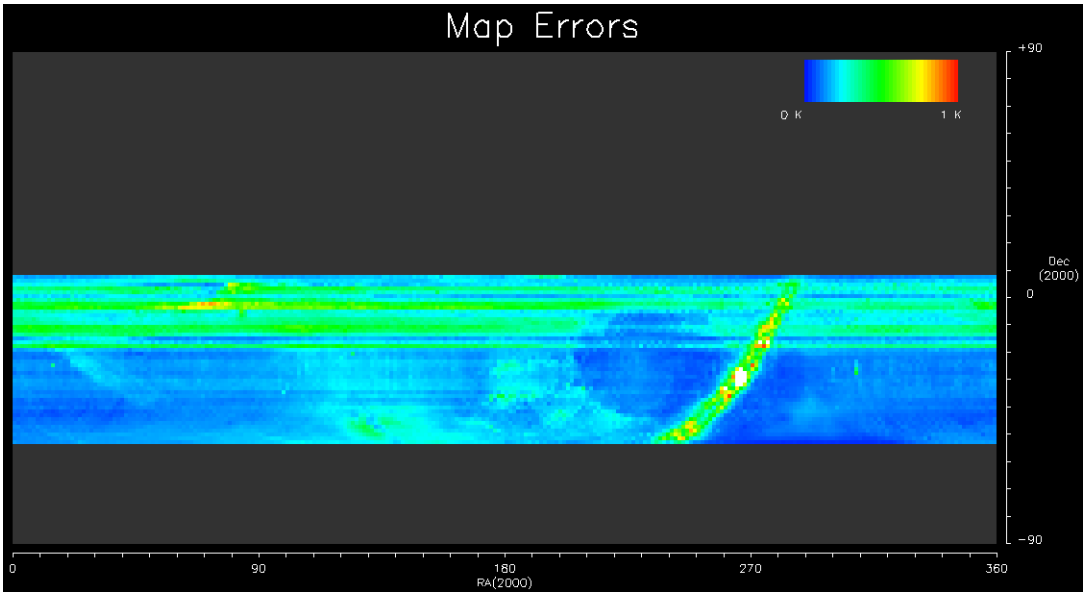

(b)

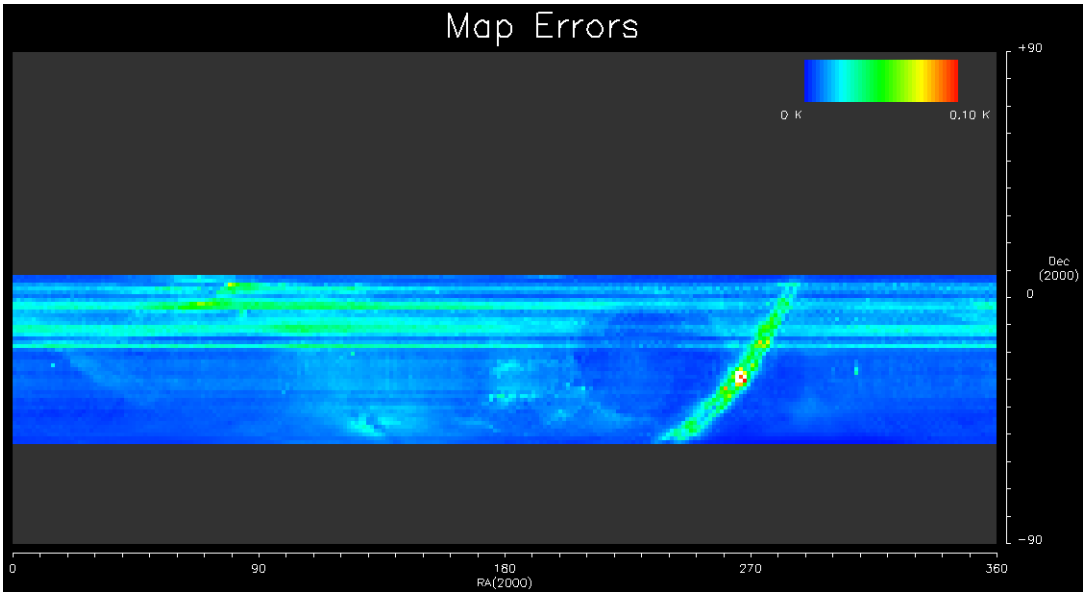

Figure 17: Error maps, showing errors as standard deviation (a) and standard deviation over root number of samples (b). Both error maps are taken from data to which a spline-fit baseline removal has been applied.

(a)

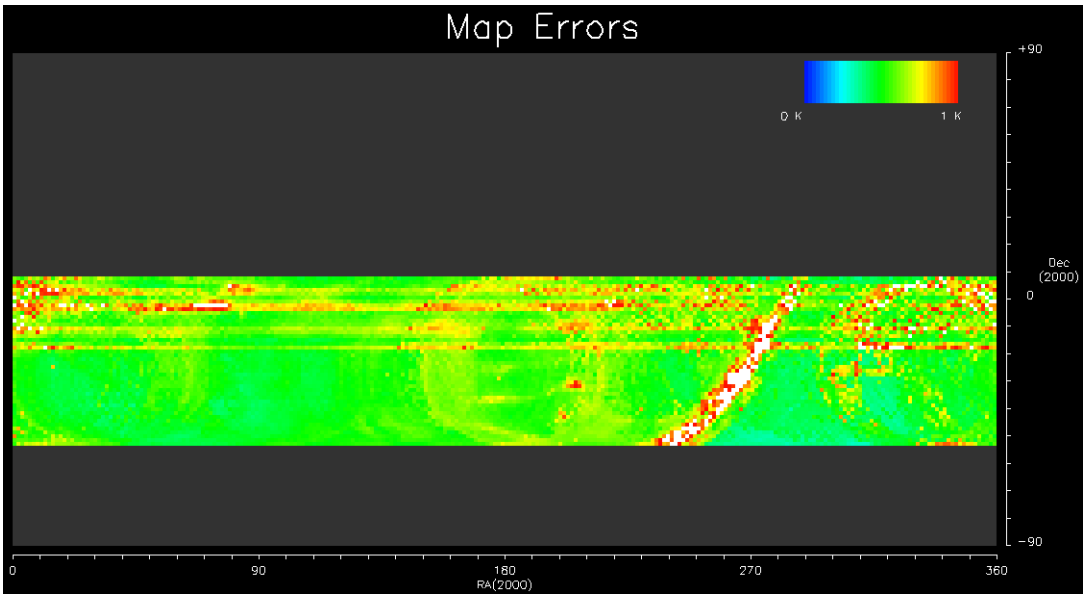

(b)

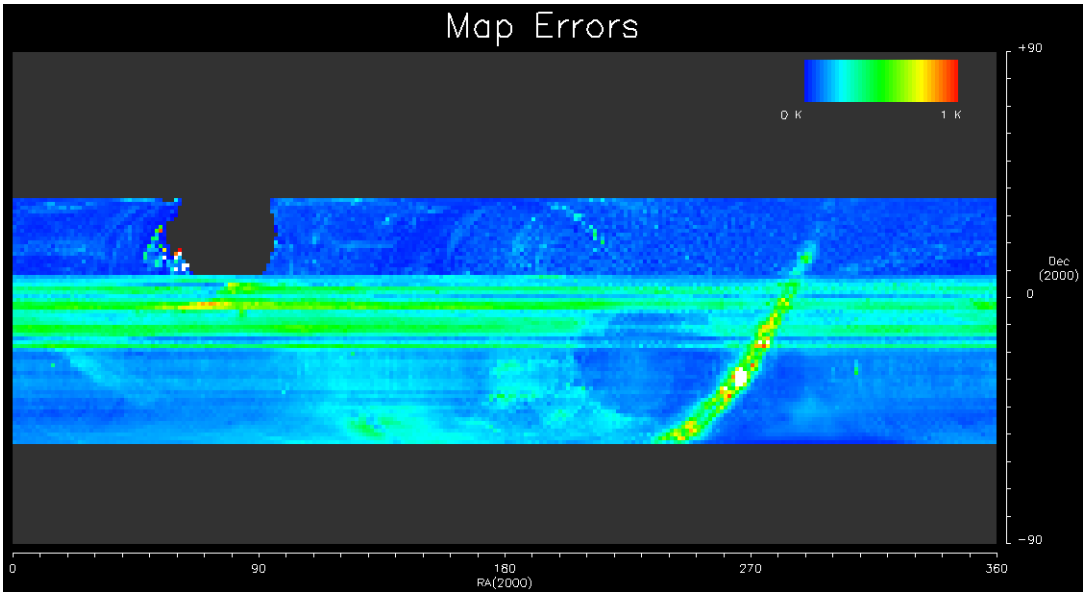

Figure 18: Error on map which doesn't have spline baseline correction (a), and error on combined map (b) that has spline baseline.

Alternatively, it could indicate that residual striping exists on larger angular scales than the more obvious striping; data is cut by azimuth near the sun, and striping is correlated with azimuth. Removing one all data from one azimuth for a pixel would eliminate the effect of striping on the standard deviation of the pixel. Finally, the double galactic plane feature seems to indicate an error in our pointing, despite the fact that pointing statistics are nominally a factor of ten better than the pixel resolution, and the anecdotal confirmation obtained by the shared features in the Brazil and Colombia maps.

Obviously, the statistics are not gaussian over the whole map. However, far from the galactic plane, in cold sky regions where the angular power at larger scales (making pointing errors less important) and away from striped regions, the error may be gaussian. As an investigation of this, we show a couple of representative pixels (including only Brazil data) individually. Figure 19 shows a pixel from a clean sky region ($\alpha = 28\delta = -42$), both before and after a spline baseline has been subtracted. The statistical error of the pixel, after baseline, is $6.1mK$. This figure clearly shows the need for using the spline baseline. Figure 20 shows a pixel that has residual striping. Figure 21 shows the expected rank of the hits of the pixels, determined from the (midrange) mean, versus actual rank. If the data were normally distributed, the graph would be a straight line. The S-shape of the clean pixel shows a normally distibuted midrange, with outliers. The dirty pixel shows poorer statistical properties, as expected.

The following table summarizes some statistics:

Statistic	**Value**
Sky Coverage	$\sim 70\%$
ΔT (minimum)	$5mK$
Gain	$48.07KV^{-1} \pm \sim 16\%$
T_{rec}	$57.37K \pm \sim 8\%$
Base. Suscep. Temp.	$-0.022VK^{-1} \pm \sim 10\%$
HPBW (x-dir)	$2.46 \pm \sim 1\%$ degrees
HPBW (y-dir)	$2.92 \pm \sim 1\%$ degrees
Ω_{beam}	$8.16 \pm 2\%$ square degrees

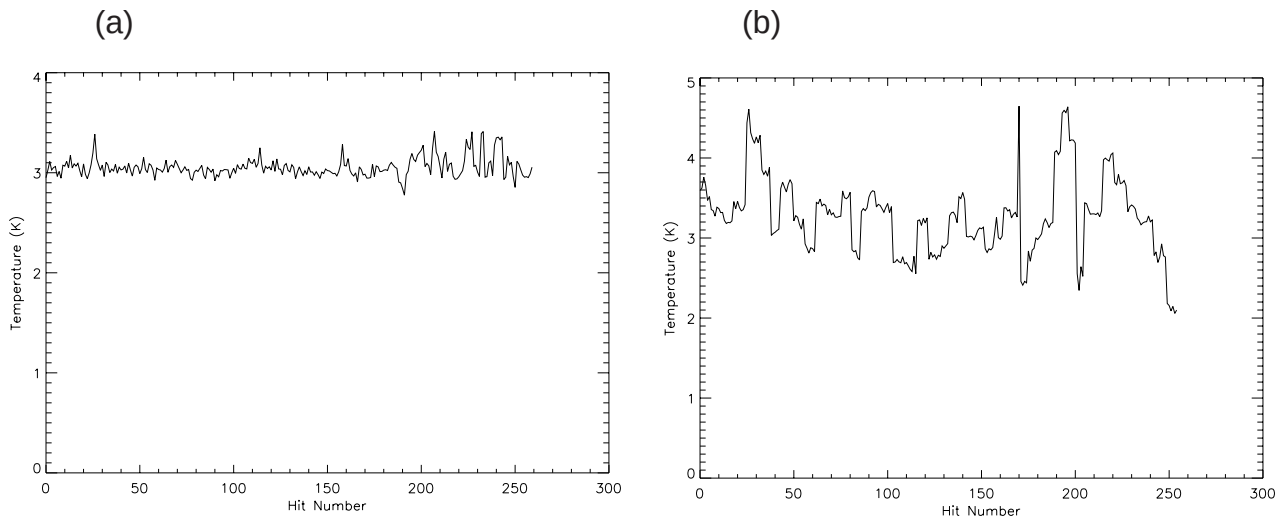

Figure 19: Pixel from clean region of sky. Pixel after spline baseline is shown in (a). Before spline baseline is shown in (b), exhibiting the effect of low-frequency noise. The higher dispersion of data taken in november is seen at the end of the pixel. This could be from atmospheric effects, since november is a humid summer month in brazil.

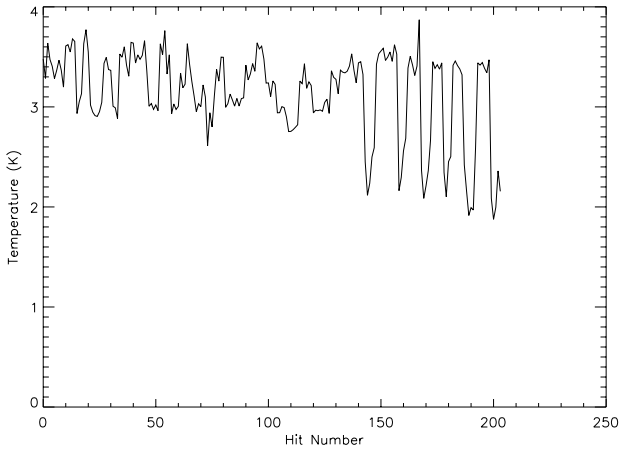

Figure 20: Pixel from a groundstriped declination band). The correlation with azimuth is clearly seen; adjacent sections of the data with different means come from different azimuths.

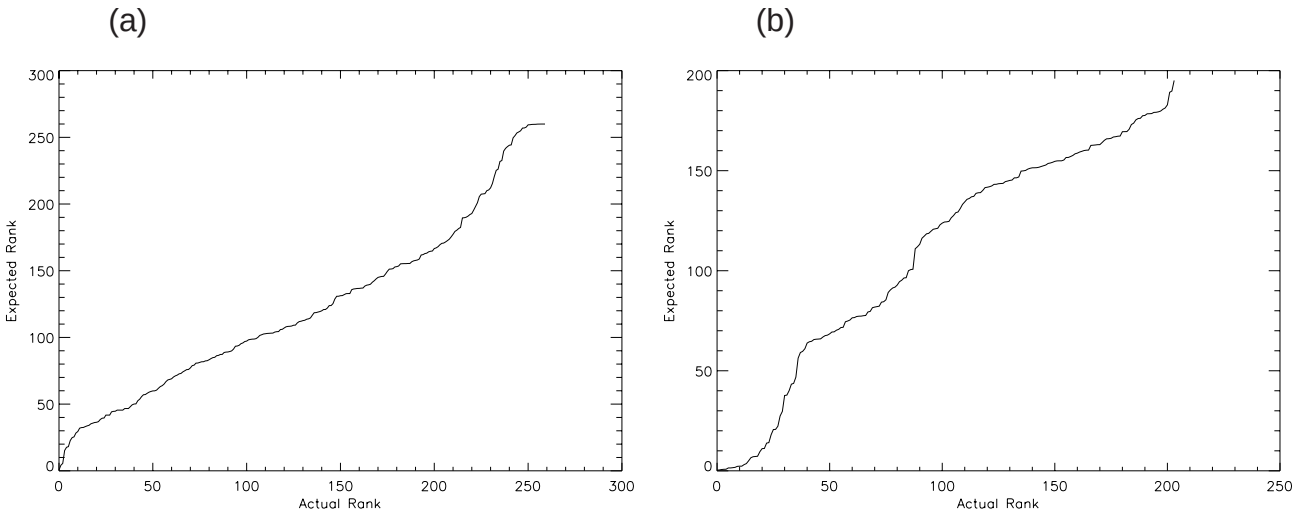

Figure 21: Rank plots of the clean (a) and dirty (b) pixel.

5 Conclusions

At this point it would be a good idea to review the qualities necessary for a "good" map, and see how our data meets or fails to meet the criteria:

1. **Receiver gain.** Receiver gain was not calibrated to better than 15 %. This error is due primarily to uncertainty in the characterization of the beam pattern and the signal when the beam was centered on the moon. The uncertainty in gain could be reduced to the $\sim 4\%$ to which the radio temperature of the moon is known.

2. **Accurate determination of the zero-level of the map.** Unfortunately we cannot formally claim an absolutely calibrated zero-level, because our determination of system temperature relied on prior knowledge of the spatial variation of galactic emission, based on the Banday "cold region." We could not even make accurate relative calibration of the system temperature, due to uncertainty in the beam pattern.

3. **Control of baseline errors.** We have had moderate success in removing 1/f noise from our maps. We are confident that we can improve the situation further with a backwards correction on our spline baseline fit. Ground striping still degrades our baseline considerably, although some regions of our map appear free of this effect. In the future, improved ground shields should reduce striping

considerably, and taking data at two zenith angles should allow striping to be further removed in data analysis.

4. **Full sky coverage.** We have covered approximately 70% of the sky. Since the apparatus is now in Brazil, the improvements I discussed will not affect the data taken in Colombia. However, Colombia data did not show ground striping, so if our method of relative calibration holds, Colombia data could still be useful.

An additional error that does not fit into the above categories is pointing error. However, we should be able to resolve this issue with existing data.

Two areas stand out above all else as in need of improvement, these being ground contamination and system parameter determination. A better determination of gain is achievable by a more thorough characterization of the system's response to the moon. System temperature will also be aided by this. In addition, a system test using a liquid nitrogen target would help constrain system temperature. If a hot target (eg using anechoic material) could be used effectively, we could also contrain gain. Ground striping could be removed by taking data at two zenith angles, and especially by use of improved ground shields. It seems especially important to determine if the stationary signal is indeed ground contamination; if it is not, dealing with it may require a different approach, even a change of site.

Although current data does not live up to the expectations of the GEM project, this analysis has been useful in pointing out shortcomings that can be resolved. All of the above mentioned areas of improvement are feasible with not too much effort or cost. Some of them have already been implemented. Data taking should resume this season, and we have reason for cautious optimism about forthcoming results.

6 Acknowledgements

First, I would like to thank Dr. Smoot for providing me with the opportunity to do this research. Working for Dr. Smoot has been a very educational experience for me. I think that the opportunity for independent thought and self-reliance is not found everywhere in the undergraduate research experience. And thanks for sending me to Brazil.

Special thanks must go to Camilo Tello, for guiding us through the early stages of the data analysis, and for helping us with the later stages. Thanks also for providing general support and guidance. And especially thanks for taking the data.

Thanks to Domingos Barbosa, for his support and his sense of humor.

Last but not least thanks to Arman, Nish and Kate, for their hard work and their good company.

May Kate, Kevin, Anjuli, Yaniv and Rui have as much fun as we did.

References

[1] Banday, A.J. *Fluctuations in the Cosmic Microwave Background*, PhD thesis 0ct. 13 1992

[2] Heafner, P.J. *Fundamental Ephemeris Computations*, Willman-Bell 1999

[3] Lo, Y.T. and Lee, S.W. ed., *Antenna Handbook Volume 2*, Van Nostrand Reinhold 1993

[4] Kraus, J.D. *Radio Astronomy*, McGraw-Hill 1966

[5] Tegmark, M. et al, *astro-ph/9905257*

[6] Krotikov, V.D. and Pelyushenko, S.A., *Soviet Astronomy* Vol. 31, No. 2, Mar.-Apr. 1987

[7] Knox, L., *astro-ph/9811358*

[8] Delabrouille, J., *Asron. Astrophys. Suppl. Ser.* 127 555-567 (1998)

[9] De Zotti, G. et al, *astro-ph/9902103*

[10] Platania, P. et al, *astro-ph/9707252*

[11] O'Neil, K., *astro-ph/0203001*

[12] Longair, M., *High Energy Astrophysics v.2*, Cambridge University Press (1992)

[13] Haslam, C.G.T. et al, *Astr. Ap.*, 100, 209 (1982)

[14] Reich, P. and Reich, W., *Astr. Ap. Suppl.*, 63, 205 (1986)

[15] Jonas, J.L. et al, *M.N.R.A.S.*, 289, 505 (1998)

[16] *http://ssd.jpl.nasa.gov/horizons.html*